Bioinspired Composite Microfibers for Skin Adhesion and Signal Amplification of Wearable Sensors

*Dirk-M. Drotlef, Morteza Amjadi, Muhammad Yunusa, and Metin Sitti**

A facile approach is proposed for superior conformation and adhesion of wearable sensors to dry and wet skin. Bioinspired skin-adhesive films are composed of elastomeric microfibers decorated with conformal and mushroom-shaped vinylsiloxane tips. Strong skin adhesion is achieved by crosslinking the viscous vinylsiloxane tips directly on the skin surface. Furthermore, composite microfibrillar adhesive films possess a high adhesion strength of 18 kPa due to the excellent shape adaptation of the vinylsiloxane tips to the multiscale roughness of the skin. As a utility of the skin-adhesive films in wearable-device applications, they are integrated with wearable strain sensors for respiratory and heart-rate monitoring. The signal-to-noise ratio of the strain sensor is significantly improved to 59.7 because of the considerable signal amplification of microfibrillar skin-adhesive films.

Considerable attention is being paid to wearable medical systems owing to their seamless integration with the human body and prolonged recording of physiological activities.[1–3] Continuous monitoring of important vital signs, such as respiratory rate, heart rate, body temperature, and blood pressure level, can greatly assist early diagnosis of diseases and subsequent therapy. Various wearable physical sensors, electrochemical transducers, and transdermal drug delivery systems have been developed by the incorporation of functional nanomaterials into flexible supporting materials.[4–17] Recently, it has been shown that multifunctional wearable systems can accomplish simultaneous sensation and on-demand release of therapeutic compounds.[18–20] Despite remarkable advances have been made in wearable medical devices, their conformal attachment to the rough, curvilinear, soft, and textured surface of the skin remains a grand challenge.[15,20,21] In fact, strong adhesion between wearable systems and skin is required for noise-free, sensitive, and accurate monitoring of body signals.

Nature can offer alternative strategies for strong and reliable adhesion to complex surfaces. For instance, geckos can adhere to rough surfaces with their adhesive pads consisting dense arrays of fine hairs or starfishes stick to complex underwater surfaces through chemical glue secretion.[22,23] Inspired by such biological systems, chemical adhesives,[24] gecko-inspired microfibers,[25–28] and microneedle arrays with swellable tips[29] have been proposed for strong attachment to complex surface topographies. However, their adhesion performance on skin is still questionable. For example, adhesives based on chemical bonding can irritate the skin and cause pain during their removal. Although gecko-inspired adhesive fibers demonstrate strong and reversible adhesion on smooth surfaces, their adhesion on slightly rough and soft surfaces is poor.[30–32] On the other hand, microneedle arrays with swellable tips require harmful skin piercing for suitable adhesion.[29] Recently, alternative approaches, such as microfibers with soft tips and hard fibers, low modulus and miniaturized suction cup designs, adhesive composite materials, and ultrathin packaging have been pursued to enhance the skin adhesion.[14,20,32–37] However, they often need complex, multistep, and time-consuming microfabrication processes. Thus, it is highly desirable to have conformal and reliable skin adhesion through a facile, cost-effective, and mass-producible method.

Herein, we propose a facile method for superior conformation and adhesion of bioinspired composite microfibers to the hierarchical topography of soft and textured skin. The proposed soft and stretchable skin-adhesive micropatterns are composed of poly(dimethylsiloxane) (PDMS) microfibers decorated with conformal and mushroom-shaped vinylsiloxane (VS) tips. We show that crosslinking of the viscous VS tips directly on the skin surface can greatly enhance the skin adhesion through their excellent shape conformation to the multiscale roughness of the skin. High adhesion strength of 18 kPa is achieved after optimizing the pattern geometries and processing parameters of skin-adhesive films. As a wearable device application of our skin-adhesive films, we integrate them with wearable strain sensors for respiratory and heart-rate monitoring. The signal-to-noise ratio (SNR) of the strain sensor is significantly improved to 59.7 because of the considerable enhanced signal transfer of microfibrillar skin-adhesive films.

Figure 1A illustrates the fabrication process of skin-adhesive microfibrillar films (see the Experimental Section in the Supporting Information for details). Briefly, the liquid PDMS precursor solution was first cast onto a PDMS mold with cylindrical cavities (step i). The excess PDMS was removed with a bar coater in order to obtain a 200 μm thick backing layer (step ii). After curing the PDMS precursor solution, uniformly shaped cylindrical microfibers were obtained upon demolding (steps iii–iv) (see Figure S1 in the Supporting Information).

Dr. D.-M. Drotlef, M. Amjadi, M. Yunusa, Prof. M. Sitti
Physical Intelligence Department
Max Planck Institute for Intelligent Systems
Stuttgart 70569, Germany
E-mail: sitti@is.mpg.de
M. Amjadi, Prof. M. Sitti
Max Planck-ETH Center for Learning Systems
Max Planck Institute for Intelligent Systems
Stuttgart 70569, Germany

DOI: 10.1002/adma.201701353

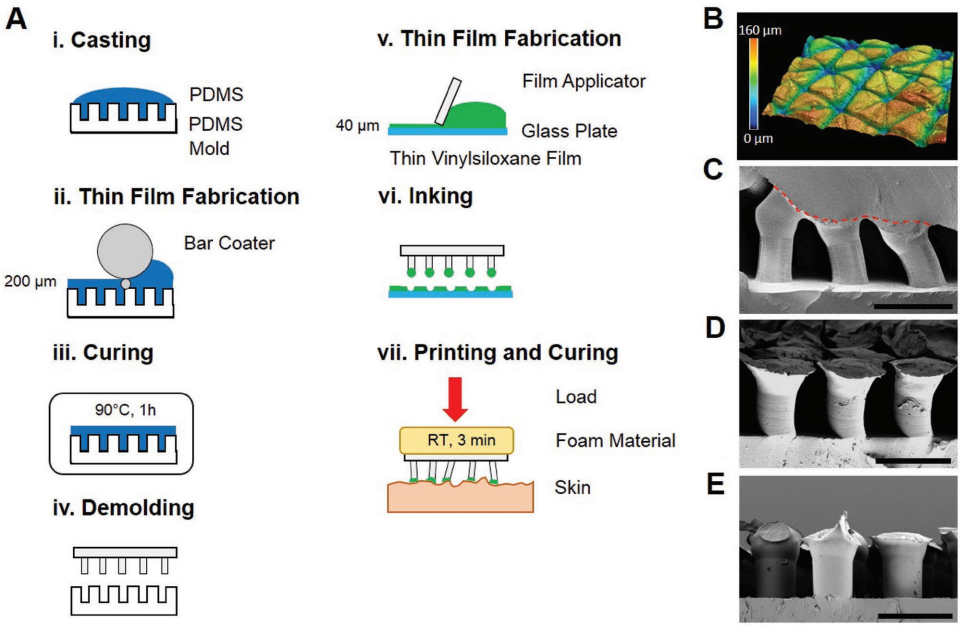

Figure 1. A) Fabrication process of the skin-adhesive films; fabrication of the PDMS microfiber film (steps i–iv), inking and printing process for the conformal attachment to the skin (steps v–vii). B) 3D laser-scanning microscopy image of the skin surface in the biological human forearm, revealing island-like planar areas and interconnected microgrooves of the skin surface. C) Cross-sectional SEM image of an adhesive film attached to an artificial skin replica; the red dashed line indicates the interface between the skin-adhesive film and artificial skin. D) Cross-sectional SEM image of an adhesive film after its detachment from a planar area of the skin, showing mushroom-shaped fibers with optimally shaped tips. E) Cross-sectional SEM image of microfibers showing the conformation of different fiber tips on different locations on the skin; the second fiber is detached from microgrooves of the skin surface while the third one conformed to a planar area. Scale bar: 100 µm.

A thin and homogeneous layer of the VS precursor solution was next coated over a glass plate by a film applicator (step v). After partial crosslinking (pre-crosslinking) of the VS layer, the micropatterned PDMS film was manually inked onto the thin layer, leading to the selective transfer of the viscous VS onto microfiber tips (step vi). The microfibers decorated with viscous VS tips were applied on the skin surface. A soft foam was then placed on the backside of the micropatterned film and a preload was applied to ensure conformal contact of the viscous VS tips to the hierarchical skin topography (step vii). Within a few minutes, the viscous VS was directly crosslinked on the skin surface, leading to a strong skin adhesion. It should be noted that we utilized PDMS for the fabrication of microfibers due to its slow crosslinking and low viscosity, enabling PDMS microstructures with optimal shapes and homogeneous micropatterns. The fast crosslinking kinetics of the VS may cause imperfect mold replication, leading to shallow concave and convex micropatterns.[38]

We selected VS as our skin interfacing material due to its several features that can influence the skin adhesion. First, VS is developed and approved for biomedical applications (e.g., forming dental impressions). In fact, neither its individual components (base and catalyst) nor the precursor solution cause any biocompatibility issues. Therefore, it prevents skin or tissue irritation even after direct crosslinking on the skin. Second, this two-component material possesses much faster crosslinking kinetics than other elastomers, such as PDMS and Ecoflex. Consequently, it can be fully crosslinked within a few minutes at room temperature. Third, its suitable viscosity enables successful transfer-patterning process and texture/roughness conformation. Last, it belongs to the family of silicone rubbers and allows covalent bonding with base PDMS microfibers.

3D laser-scanning microscopy images of the skin surface in the forearm revealed that the skin possesses dual-scale roughness (from the micro- to the nanoscale) (see Figure 1B and Figure S2 in the Supporting Information). Moreover, the skin surface is composed of island-like planar areas with an averaged surface roughness of 0.4 µm separated by interconnected microgrooves having vertical roughness of around 104.2 µm. In fact, one of the main skin-adhesion challenges is conformation to high and multi-length-scale roughness of the skin surface. Figure 1C illustrates a representative cross-sectional scanning electron microscopy (SEM) image of a composite microfiber adhesive film attached to a skin replica, showing conformal interfacing between the adhesive film and skin replica. Furthermore, PDMS microfibers act as load-transferring components while crosslinked VS tips provide a strong adhesion to the skin. Figure 1D,E depicts the surface morphology of the adhesive film when it was detached from the skin. As shown in Figure 1D, mushroom-shaped microfibers with optimal tip shapes were formed when the viscous VS was directly crosslinked on the planar area of the skin. Additionally, the viscous VS completely filled the space of the skin microgrooves prior to its crosslinking (Figure 1E). Therefore, our micropatterned adhesive films are capable of establishing intimate contact with both micro- and nanoscale roughness of the skin.

Further experiments were carried out to optimize the structural integrity of PDMS microfibers as well as shape adaptation of the viscous VS tips by varying the aspect ratio (AR) of PDMS microfibers, applied preload pressure, layer thickness

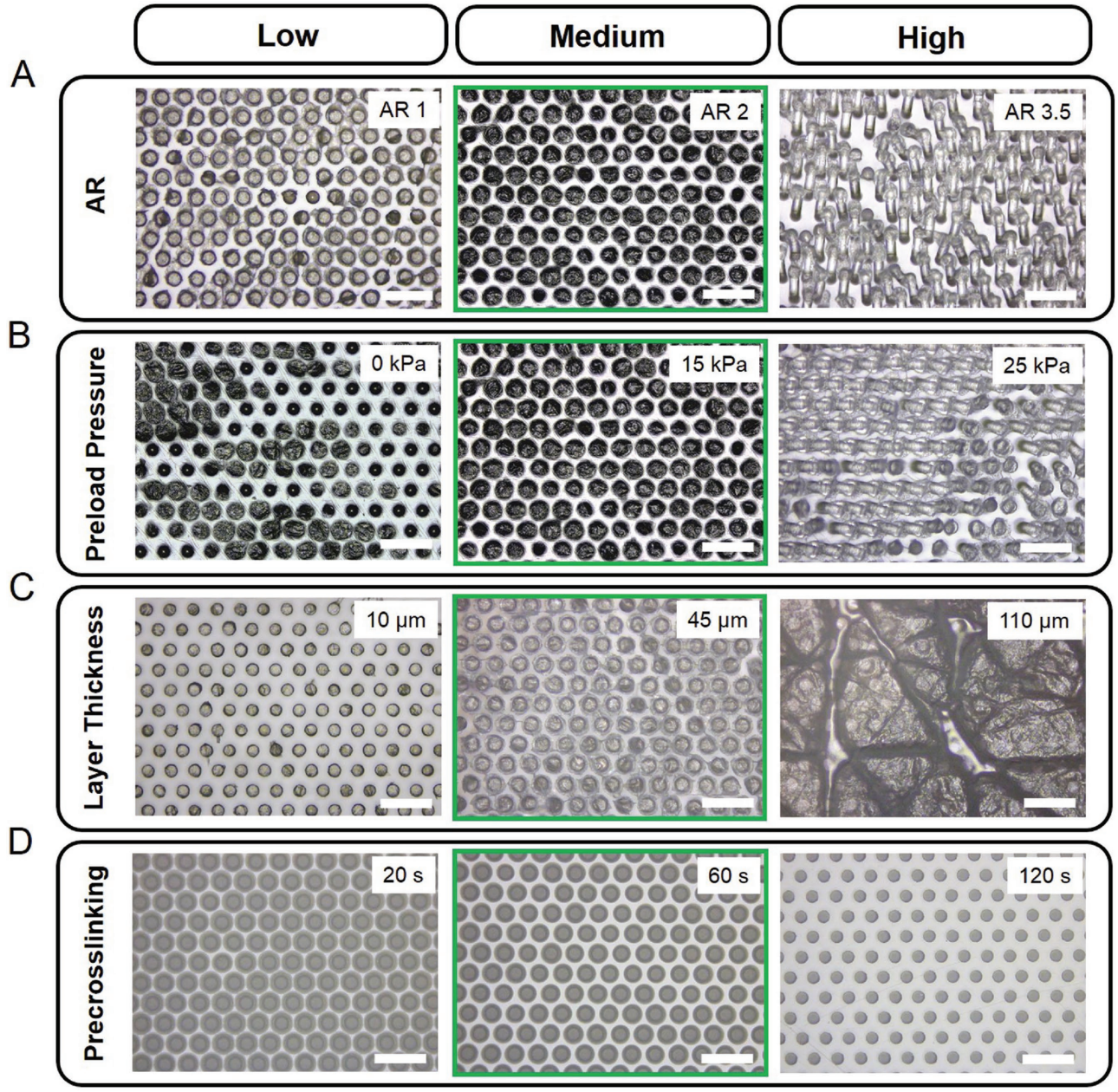

Figure 2. Optimization of the process parameters, including AR, preload pressure, layer thickness, and pre-crosslinking duration. A) Optical microscopy images of patterns with different ARs after their detachment from the skin. B) Microscopy images of patterns under different preload pressures after their detachment from the skin. C) Microscopy images of patterns inked to the viscous VS with different layer thicknesses after their detachment from the skin. D) Microscopy images of microfibers inked into VS films after different pre-crosslinking durations and then printed on flat glass slides. Optimal process parameters are indicated with green borders. Scale bar: 200 µm.

of the viscous VS, and pre-crosslinking duration. To this end, we imaged the surface topology of all adhesive samples and exploited the possible buckling/collapse of microfibers and contact quality of the inked tips after their complete detachment from skin and glass (see **Figure 2**, and Table S1 and Figure S3–S6 in the Supporting Information). We observed that microfibers with an AR of 2 accomplished adequate conformation to the multi-length-scale roughness of the skin by applying moderate preloads. Microfibers with an AR of 1 showed only partial contact with skin microgrooves, whereas microfibers with an AR of 3.5 were buckled even under small preloads due to their insufficient bending stiffness (see Figure 2A and Figure S3 in the Supporting Information). On the other hand, a moderate preload pressure of 15 kPa appeared to be the optimal value for micropatterns made of microfibers with an AR of 2, enabling them to fully contact the skin roughness. As shown in Figure 2B, homogeneous and large mushroom-shaped VS tips were formed when a preload of 15 kPa was applied to a skin-adhesive film. In contrast, small and spherical crosslinked VS tips were formed under insufficient preload, and micropatterns

were partially or completely collapsed when the preload pressure exceeded 20 kPa (see Figure 2B and Figure S4 in the Supporting Information).

The viscous VS film with layer thickness in the range of 35–45 μm resulted in homogeneous and large mushroom-shaped tips (Figure 2C). For thinner layers, however, the transferred viscous VS to microfiber tips was small and insufficient for strong skin adhesion (see Figure 2C and Figure S5 in the Supporting Information). Furthermore, microfibers were fully immersed into the viscous VS film when the layer thickness approached or surpassed the fiber height. Additionally, we found that 30–60 s was the ideal pre-crosslinking time range for high-throughput inking and transfer-patterning process (see Figure 2D and Figure S6 in the Supporting Information). For shorter pre-crosslinking time, the initial viscosity was low and the amount of the transferred viscous VS to microfiber tips was large, leading to connected tips. On the other hand, the viscosity was high for long pre-crosslinking duration and no VS was transferred to microfiber tips (see Figure 2D and Figure S6 in the Supporting Information).

To quantitatively analyze the adhesion performance of our adhesive films, circular-shaped adhesive samples with 1 cm^2 area were attached onto the human skin in the forearm area and their force–displacement curves were measured by a customized adhesion setup (see **Figure 3**A and Figure S7 in the Supporting Information). Figure 3B illustrates the force–displacement curves for a PDMS microfiber array with an averaged VS mushroom-shaped tip diameter of 95 μm (see the inset of Figure 3B). For comparison, we also measured the adhesion performance of an unstructured sample (i.e., a flat PDMS film attached to the skin via the VS interfacing layer) (see the inset of Figure 3B). The preload pressure, thickness of the viscous VS layer, and crosslinking time were kept the same for both samples. The adhesion force (F_{off}) for microfibrillar and unstructured samples was 1.7 and 0.7 N, respectively, showing significant enhancement of the skin adhesion using microfibrillar adhesive films. The high-adhesion performance of mushroom-shaped fibers originates from more uniform stress distribution at the microfiber tip interfaces.[39–42] Longer retraction distance of the microfibrillar sample before its detachment from the skin further confirms the improved load sharing of mushroom-shaped fibers. Figure 3C illustrates the adhesion strength of microfibrillar adhesive films with different VS tip diameters. The VS tip diameter was controlled by tailoring the layer thickness of the viscous VS film. The adhesion strength was dependent on the tip diameter. Furthermore, the micropatterned adhesive films with larger VS tip sizes produced higher adhesion strength. The maximum adhesion strength of 18 kPa was achieved by a microfiber array with an averaged VS tip diameter of 95 μm. The higher adhesion strength of microfibers with larger VS tips is attributed to their optimized geometry and subsequent improved load sharing due to their enhanced roughness and texture conformation.[27,28,40]

To confirm the remarkable adhesion improvement of our adhesive films through crosslinking of the viscous VS tips directly on the skin, we measured the adhesion strength of a microfibrillar PDMS film with crosslinked VS mushroom-shaped tips. The adhesion strength of the adhesive film directly crosslinked onto the skin surface was 200 times higher than that of the microfibrillar PDMS sample, where mushroom-shaped tips were fully crosslinked before their application to the skin (see Figure S8 in the Supporting Information). This significant improvement in the skin adhesion is due to the high shape conformation of the viscous VS tips to the skin surface prior to their complete crosslinking. The reusability of our adhesive films was tested by multiple times inking and printing of a microfibrillar adhesive film. The adhesion strength of the sample was 14, 10, and 8 kPa for first, second, and third time inking, respectively. Indeed, the adhesion strength approached to that of the unstructured sample after three cycles of inking (Figure 3H). Moreover, more crosslinked VS was accumulated on the microfiber tips during each inking and printing cycle and a partial or complete VS film was formed on microfibers, degrading the contribution of mushroom-shaped fibers to the adhesion improvement of the adhesive film (see Figure 3I–K). Additional experiments were conducted to investigate the durability and biocompatibility of the fabricated skin-adhesive films. Both microfibrillar and unstructured samples were attached to the skin in the human forearm and subjected to repeated bending–straightening cycles. The microfibrillar skin-adhesive film exhibited a robust skin adhesion under more than 300 loading cycles, while the unstructured sample started to partially detach from the skin after 100 cycles (see Figure S9 in the Supporting Information). After cyclic loading test and detachment of the microfibrillar adhesive film from the skin, no irritation was observed on the skin surface. Possible skin irritation of the microfibrillar adhesive film upon prolonged use was further studied. There was no skin irritation when a micropatterned adhesive film was mounted onto the skin for over 24 h (see Figure S9 in the Supporting Information). Notably, our microfibrillar adhesive films could also adhere to the wet skin surface with high adhesion strength and durability (see Figure S10 in the Supporting Information). Therefore, our composite microfibrillar skin-adhesive films could provide strong skin adhesion with high durability and minimal irritation.

We demonstrated the utility of our skin-adhesive films by integrating them with flexible strain sensors for detection of tiny skin deformations. Silver nanoparticle (AgNPs) thin film-based strain sensors were fabricated on the top of the micropatterned PDMS films (see Figure S11 and the "Skin-Adhesive Strain Sensor" section in the Supporting Information for the detailed fabrication process). The integrated skin-adhesive sensors were highly flexible and could easily be attached onto the skin (**Figure 4**A). Figure 4B illustrates the electromechanical behavior of a strain-sensor prototype under repeated stretching–releasing cycles. The strain sensor was subjected to sawtooth strain profiles with a frequency of around 1.8 Hz while its resistance was simultaneously recorded. The strain sensor could precisely measure strains from 0.1% to 1% with significant resistance changes. The gauge factor (GF) of the strain sensor—relative change of the resistance divided by the applied strain—in the linear range of 0%–1% was around 767, showing ultrahigh sensitivity of strain sensors. The ultrahigh GF of the strain sensor was attributed to the microcrack opening–closing mechanism of AgNP thin films under stretching–releasing cycles (see Figure S12 in the Supporting Information).[1,6]

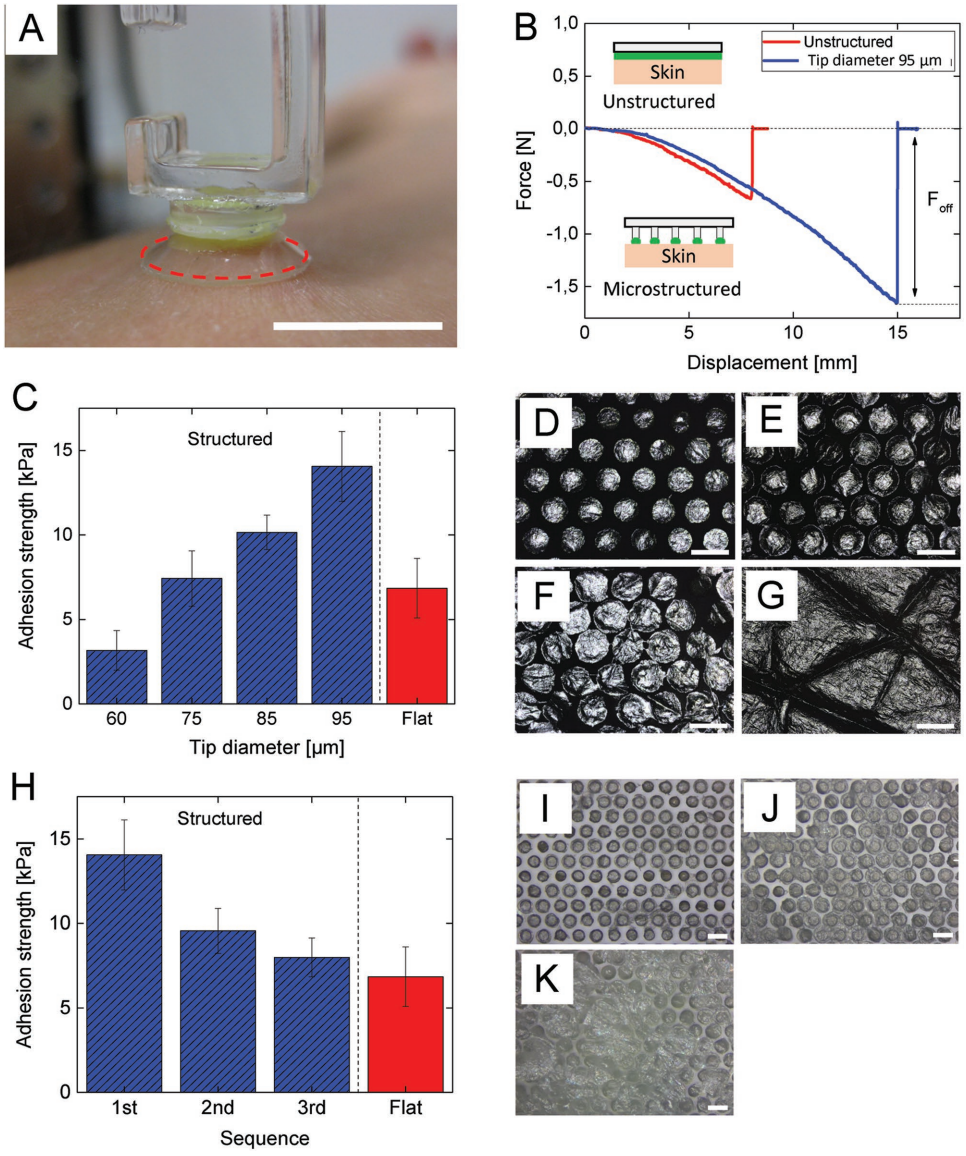

Figure 3. Force–displacement curves and adhesion measurements of the composite microfibrillar adhesive films attached to the skin. A) Photograph of an attached skin-adhesive film to the biological human forearm during the retraction cycle of the adhesion experiment; dashed red line indicates the interfacing border between the adhesive film and the skin. Scale bar: 1 cm. B) Force–displacement curves of a micropatterned adhesive film with an averaged VS tip diameter of 95 µm (blue curve) and an unstructured sample (red force curve). C) Adhesion strength of micropatterned adhesive films with different VS tip diameters and unstructured samples directly measured on the skin. D–G) Microscopy images of the corresponding samples with an averaged tip diameter of D) 60 µm, E) 85 µm, F) 95 µm, and G) the unstructured sample. Scale bar: 100 µm. H) Adhesion strength of skin-adhesive films after multiple inking and attachment process. I–K) Top-view optical microscopy images of microfibers after I) first, J) second, and K) third attachment cycles. Scale bar: 100 µm.

Figure 4C shows the response of a microfibrillar skin-adhesive strain sensor attached to the human chest area. The resistance of the sensor rapidly increased/decreased upon inhalation/exhalation due to the expansion/shrinkage of the chest during respiration. Furthermore, the microfibrillar skin-adhesive strain sensor could distinguish normal and deep respirations with a considerable signal difference. Real-time detection of abnormal respiration rate and temporal patterns can help early diagnosis of several diseases such as asthma, hearth failure, embolism, and so on.[43,44] The inset of Figure 4D depicts a microfibrillar skin-adhesive strain sensor mounted on the radial artery of the wrist. The strain sensor was strongly bonded to the skin owing to the high adhesion strength of our composite microfibrillar adhesive film. There was no detachment or delamination of the sensor on the skin even under large straining conditions. Figure 4D illustrates a record of the blood-flow pulse over one minute, showing the heart rate with the frequency of 84 beat per minute. Although there were changes in the base resistance of the sensor due to hand movements, the sensor could record the blood-flow pressure with high sensitivity. Figure 4E depicts the response of the skin-adhesive sensor

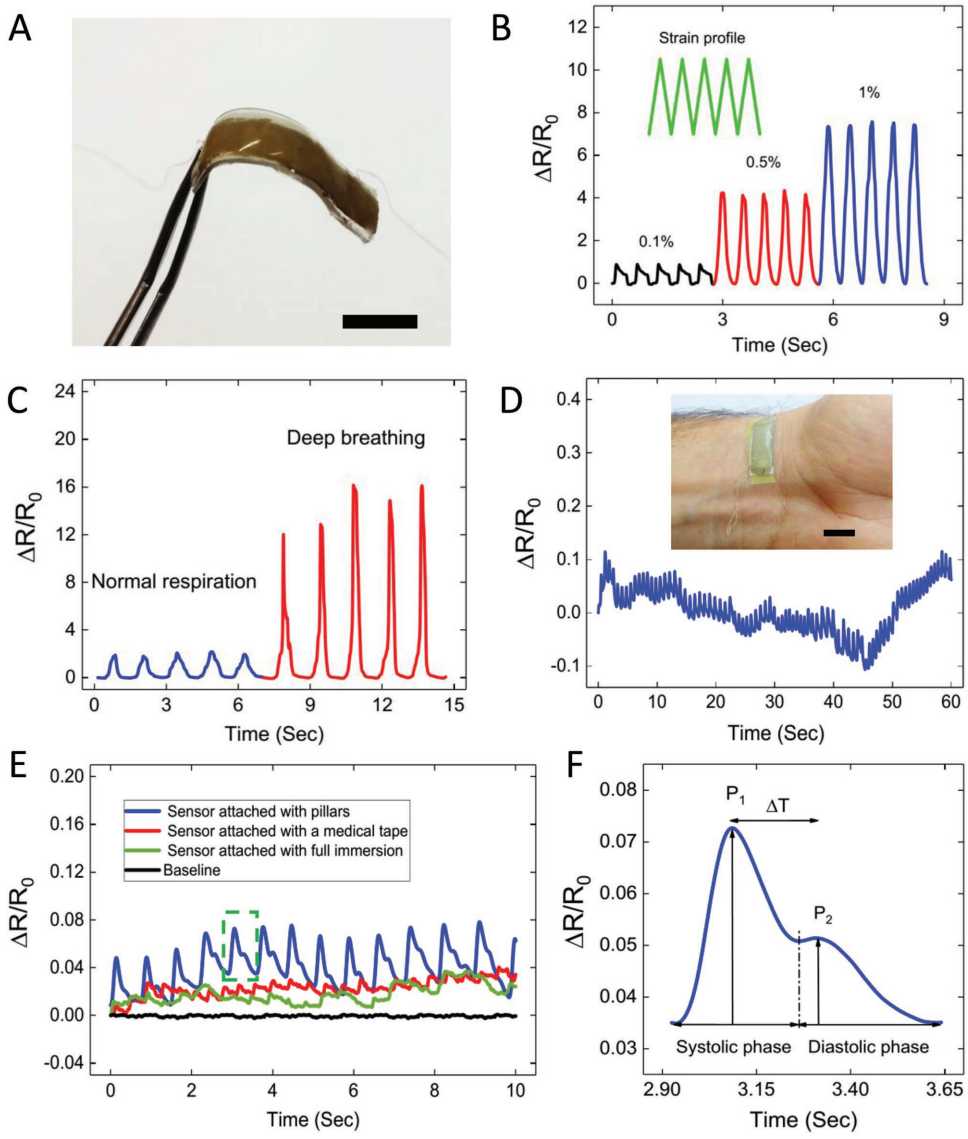

Figure 4. Wearable skin-adhesive strain sensors for healthcare applications. A) Photograph of a strain sensor fabricated on the top of a microfibrillar adhesive film, showing high flexibility of the device. B) Electromechanical response of a strain sensor to the dynamic stretching–releasing cycles. C) Response of a microfibrillar strain sensor attached to the human chest area, indicating sharp increase of the resistance upon deep inhalation. D) Output signal of a microfibrillar strain sensor mounted onto the radial artery of the wrist; the inset, photograph of the strain sensor attached to the wrist through inking and printing process. E) Output signal of the strain sensor mounted onto the radial artery of the wrist with different attachment methods (attaching by a commercial medical tape, microfibrillar adhesive film with mushroom-shaped VS tips, and microfibrillar adhesive film fully immersed into a flat VS film); the dashed green box represents the output signal of the sensor during one cardiac cycle. F) Response of the strain sensor during one cardiac cycle (the dashed green box), clearly showing systolic and diastolic phases and peaks. Scale bar: 1 cm.

for 10 s, clearly indicating that the waveform pattern of the artery pulse was detectable. Furthermore, both systolic and diastolic phases and peaks were successfully identified by the sensor output signal (Figure 4F). This waveform corresponds to the radial blood-flow pulse for an adult on his third decade life with a compliant vein.[45–47] The time delay between systolic and diastolic peaks (ΔT) was around 220 ms. The derived arterial stiffness index (S.I. = volunteer height/ΔT) and reflection index (R.I. = $P_2/P_1 \times 100$) were around 7.5% and 43.7%, respectively, all within the normal range of a healthy person.[1,48–50]

We further investigated the effect of the sensor attachment method on the output signal amplification. A microfibrillar skin-adhesive strain sensor was mounted onto the radial artery of the wrist by a commercial pressure-sensitive medical tape, micropatterned PDMS with VS tips, and micropatterned PDMS fully immersed into the 100 μm thick flat VS film. To avoid stiffening of the skin-adhesive sensor, only two ends of the sensor were attached to the skin by the medical tape.

The contact spot of the sensor was maintained identical to minimize possible signal variations. As shown in Figure 4E, small peaks appeared in the sensor output when the sensor

was attached by the medical tape, indicating a weak transfer of the skin deformation to the sensor because of the poor contact area and insufficient adhesion of the bare microfibers. On the other hand, our microfibrillar skin-adhesive films with VS tips showed maximum signal transfer to the strain sensor due to their higher flexibility, arrayed micropillar structure, and strong attachment of individual microfibers to the skin surface.[15] Irregular waveform patterns were recorded once the sensor was mounted onto the skin with fully immersion process. This low signal quality is believed to be due to the reduced flexibility of the solidified VS film, making to whole sensor structure stiffer. Indeed, microstructured sample with VS tips was softer than the fully immersed sample due to the contact splitting between VS tips, leading to enhanced signal transfer.

To quantitatively assess the signal enhancement of the strain sensor attached by microfibrillar adhesive films, we calculated the SNR of the sensor as:[15]

$$\mathrm{SNR} = \mathrm{avg}(\Delta R) / \sigma_{\mathrm{baseline}} \quad (1)$$

where avg (ΔR) is the averaged resistance change of the sensor during radial pulse measurements and $\sigma_{\mathrm{baseline}}$ is the standard deviation of the baseline signal where no strain is accommodated by the sensor. The SNR of the strain sensor attached by our micropatterned adhesive films, medical tape, and fully immersion method was 59.7, 10.2, and 8.3, respectively. The significant improvement in the SNR of the strain sensor is due to the high adhesion strength of our micropatterned adhesive films, together with their compliance and flexibility.

In summary, we presented a novel approach for high-performance skin adhesion. The high adhesion strength of the adhesive films was found to be due to the enhanced roughness and texture conformation, and the load sharing of the PDMS microfibers decorated with crosslinked VS tips. Highly flexible, conformable, and biocompatible microfibrillar skin-adhesive films were easily integrated with wearable soft strain sensors to enable their strong bonding and high signal enhancement on the skin for healthcare-monitoring applications. In addition to skin, the proposed composite microfibrillar adhesive films could attach to other surfaces with complex topographies and a wide range of surface roughness length scales under various dry and wet environmental conditions.

Supporting Information

Supporting Information is available from the Wiley Online Library or from the author.

Acknowledgements

D.-M.D. and M.A. contributed equally to this work. The authors thank to Ayça Senol for her help on microfabrication.

Conflict of Interest

The authors declare no conflict of interest.

Keywords

gecko-inspired adhesives, microfibers, skin adhesives, strain sensors, wearable sensors

Received: March 9, 2017
Revised: March 31, 2017
Published online:

[1] M. Amjadi, K. U. Kyung, I. Park, M. Sitti, *Adv. Funct. Mater.* **2016**, *26*, 1678.
[2] T. Q. Trung, N. E. Lee, *Adv. Mater.* **2016**, *28*, 4338.
[3] K. Takei, W. Honda, S. Harada, T. Arie, S. Akita, *Adv. Healthcare Mater.* **2015**, *4*, 487.
[4] M. Amjadi, A. Pichitpajongkit, S. Lee, S. Ryu, I. Park, *ACS Nano* **2014**, *8*, 5154.
[5] M. Amjadi, Y. J. Yoon, I. Park, *Nanotechnology* **2015**, *26*, 375501.
[6] M. Amjadi, M. Turan, C. P. Clementson, M. Sitti, *ACS Appl. Mater. Interfaces* **2016**, *8*, 5618.
[7] W. Gao, S. Emaminejad, H. Y. Y. Nyein, S. Challa, K. Chen, A. Peck, H. M. Fahad, H. Ota, H. Shiraki, D. Kiriya, *Nature* **2016**, *529*, 509.
[8] J. Kim, R. Kumar, A. J. Bandodkar, J. Wang, *Adv. Electron. Mater.* **2016**, *3*, 1600260.
[9] J. Di, S. Yao, Y. Ye, Z. Cui, J. Yu, T. K. Ghosh, Y. Zhu, Z. Gu, *ACS Nano* **2015**, *9*, 9407.
[10] F. Zhang, Y. Zang, D. Huang, C.-a. Di, D. Zhu, *Nat. Commun.* **2015**, *6*, 8356.
[11] S. Yang, Y. C. Chen, L. Nicolini, P. Pasupathy, J. Sacks, B. Su, R. Yang, D. Sanchez, Y. F. Chang, P. Wang, *Adv. Mater.* **2015**, *27*, 6423.
[12] H. Park, Y. R. Jeong, J. Yun, S. Y. Hong, S. Jin, S.-J. Lee, G. Zi, J. S. Ha, *ACS Nano* **2015**, *9*, 9974.
[13] C. L. Choong, M. B. Shim, B. S. Lee, S. Jeon, D. S. Ko, T. H. Kang, J. Bae, S. H. Lee, K. E. Byun, J. Im, *Adv. Mater.* **2014**, *26*, 3451.
[14] R. C. Webb, A. P. Bonifas, A. Behnaz, Y. Zhang, K. J. Yu, H. Cheng, M. Shi, Z. Bian, Z. Liu, Y.-S. Kim, *Nat. Mater.* **2013**, *12*, 938.
[15] C. Pang, J. H. Koo, A. Nguyen, J. M. Caves, M. G. Kim, A. Chortos, K. Kim, P. J. Wang, J. B. H. Tok, Z. Bao, *Adv. Mater.* **2015**, *27*, 634.
[16] I. You, B. Kim, J. Park, K. Koh, S. Shin, S. Jung, U. Jeong, *Adv. Mater.* **2016**, *28*, 6359.
[17] P. Mostafalu, M. Akbari, K. A. Alberti, Q. Xu, A. Khademhosseini, S. R. Sonkusale, *Microsyst. Nanoeng.* **2016**, *2*, 16039.
[18] D. Son, J. Lee, S. Qiao, R. Ghaffari, J. Kim, J. E. Lee, C. Song, S. J. Kim, D. J. Lee, S. W. Jun, *Nat. Nanotechnol.* **2014**, *9*, 397.
[19] H. Lee, T. K. Choi, Y. B. Lee, H. R. Cho, R. Ghaffari, L. Wang, H. J. Choi, T. D. Chung, N. Lu, T. Hyeon, *Nat. Nanotechnol.* **2016**, *11*, 566.
[20] M. K. Choi, O. K. Park, C. Choi, S. Qiao, R. Ghaffari, J. Kim, D. J. Lee, M. Kim, W. Hyun, S. J. Kim, *Adv. Healthcare Mater.* **2016**, *5*, 80.
[21] H. Wang, G. Pastorin, C. Lee, *Adv. Sci.* **2016**, *3*, 1500441.
[22] E. Hennebert, R. Wattiez, M. Demeuldre, P. Ladurner, D. S. Hwang, J. H. Waite, P. Flammang, *Proc. Natl. Acad. Sci. USA* **2014**, *111*, 6317.
[23] A. M. Smith, J. A. Callow, *Biological Adhesives*, Springer, Berlin, Germany, **2006**.
[24] A. Mahdavi, L. Ferreira, C. Sundback, J. W. Nichol, E. P. Chan, D. J. Carter, C. J. Bettinger, S. Patanavanich, L. Chignozha, E. Ben-Joseph, *Proc. Natl. Acad. Sci. USA* **2008**, *105*, 2307.
[25] J. Cui, D. M. Drotlef, I. Larraza, J. P. Fernández-Blázquez, L. F. Boesel, C. Ohm, M. Mezger, R. Zentel, A. del Campo, *Adv. Mater.* **2012**, *24*, 4601.
[26] D. M. Drotlef, P. Blümler, A. del Campo, *Adv. Mater.* **2014**, *26*, 775.

[27] B. Aksak, K. Sahin, M. Sitti, *Beilstein J. Nanotechnol.* **2014**, *5*, 630.
[28] H. Marvi, S. Song, M. Sitti, *Langmuir* **2015**, *31*, 10119.
[29] S. Y. Yang, E. D. O'Cearbhaill, G. C. Sisk, K. M. Park, W. K. Cho, M. Villiger, B. E. Bouma, B. Pomahac, J. M. Karp, *Nat. Commun.* **2013**, *4*, 1702.
[30] H. Kasem, M. Varenberg, *J. R. Soc., Interface* **2013**, *10*, 20130620.
[31] C. T. Bauer, E. Kroner, N. A. Fleck, E. Arzt, *Bioinspiration Biomimetics* **2015**, *10*, 066002.
[32] V. Barreau, R. Hensel, N. K. Guimard, A. Ghatak, R. M. McMeeking, E. Arzt, *Adv. Funct. Mater.* **2016**, *26*, 4687.
[33] S. C. Fischer, E. Arzt, R. Hensel, *ACS Appl. Mater. Interfaces* **2016**, *9*, 1036.
[34] W. G. Bae, D. Kim, M. K. Kwak, L. Ha, S. M. Kang, K. Y. Suh, *Adv. Healthcare Mater.* **2013**, *2*, 109.
[35] Y. Liu, J. J. Norton, R. Qazi, Z. Zou, K. R. Ammann, H. Liu, L. Yan, P. L. Tran, K.-I. Jang, J. W. Lee, *Sci. Adv.* **2016**, *2*, e1601185.
[36] A. Koh, D. Kang, Y. Xue, S. Lee, R. M. Pielak, J. Kim, T. Hwang, S. Min, A. Banks, P. Bastien, M. C. Manco, L. Wang, K. R. Ammann, K. I. Jang, P. Won, S. Han, R. Ghaffari, U. Paik, M. J. Sleplan, B. Balooch, Y. Huang, J. A. Rogers, *Sci. Transl. Med.* **2016**, *8*, 366ra165.
[37] S. H. Jeong, S. Zhang, K. Hjort, J. Hilborn, Z. Wu, *Adv. Mater.* **2016**, *28*, 5830.
[38] A. del Campo, I. Álvarez, S. Filipe, M. Wilhelm, *Adv. Funct. Mater.* **2007**, *17*, 3590.
[39] G. Carbone, E. Pierro, S. N. Gorb, *Soft Matter* **2011**, *7*, 5545.
[40] G. Carbone, E. Pierro, *Small* **2012**, *8*, 1449.
[41] A. Del Campo, C. Greiner, E. Arzt, *Langmuir* **2007**, *23*, 10235.
[42] S. Kim, M. Sitti, *Appl. Phys. Lett.* **2006**, *89*, 261911.
[43] J.-M. Ramirez, C. S. Ward, J. L. Neul, *Respir. Physiol. Neurobiol.* **2013**, *189*, 280.
[44] Y. S. Lee, P. N. Pathirana, C. L. Steinfort, T. Caelli, *IEEE J. Transl. Eng. Health Med.* **2014**, *2*, 1.
[45] J. J. Oliver, D. J. Webb, *Arterioscler., Thromb., Vasc. Biol.* **2003**, *23*, 554.
[46] R. Kelly, C. Hayward, A. Avolio, M. O'rourke, *Circulation* **1989**, *80*, 1652.
[47] A. P. Avolio, M. Butlin, A. Walsh, *Physiol. Meas.* **2009**, *31*, R1.
[48] Z. Fan, G. Zhang, S. Liao, *2009 Canadian Conf. on Electrical and Computer Engineering*, IEEE, Piscataway, NJ, USA, **2009**, pp. 478–481, DOI: 10.1109/CCECE.2009.5090180.
[49] V. Prabha, P. Buhutkar, M. Bhutkar, G. Sivagami, *Int. J. Med. Res. Health Sci.* **2013**, *2*, 533.
[50] M. F. O'Rourke, J. A. Staessen, C. Vlachopoulos, D. Duprez, *Am. J. Hypertens.* **2002**, *15*, 426.

